Sea surface salinity under rain cells: SMOS satellite and in situ drifters observations

Jacqueline Boutin, Nicolas Martin, Gilles Reverdin, Simon Morisset, Xiaobin Yin, Luca R. Centurioni, Nicolas Reul

AGU PUBLICATIONS

JGR

Journal of Geophysical Research: Oceans

RESEARCH ARTICLE

10.1002/2014JC010070

Special Section:
Early scientific results from the salinity measuring satellites Aquarius/SAC-D and SMOS

Sea surface salinity under rain cells: SMOS satellite and in situ drifters observations

J. Boutin[1], N. Martin[1], G. Reverdin[1], S. Morisset[1], X. Yin[1], L. Centurioni[2], and N. Reul[3]

[1]LOCEAN, Sorbone Universités, UPMC/CNRS/IRD/MNHN, Paris, France, [2]SIO, La Jolla, California, USA, [3]IFREMER, Toulon, France

Key Points:
- Rain induced local variability of SMOS SSS confirmed to be −0.2 pss/mm/h
- Rain induced local variability of drifters SSS −0.21 (±0.14) pss/mm/h
- Rain induced variability of SMOS SSS mostly a true surface freshening

Correspondence to:
J. Boutin,
jb@locean-ipsl.upmc.fr

Citation:
Boutin, J., N. Martin, G. Reverdin, S. Morisset, X. Yin, L. Centurioni, and N. Reul (2014), Sea surface salinity under rain cells: SMOS satellite and in situ drifters observations, *J. Geophys. Res. Oceans*, *119*, 5533–5545, doi:10.1002/2014JC010070.

Received 18 APR 2014
Accepted 29 JUL 2014
Accepted article online 2 AUG 2014
Published online 28 AUG 2014

Abstract We study the signature of rainfall on S_{1cm}, the sea surface salinity retrieved from the Soil Moisture and Ocean Salinity (SMOS) satellite mission first by comparing SMOS S_{1cm} with ARGO sea surface salinity measured at about 5 m depth in the Intertropical Convergence Zone (ITCZ) and in the Southern Pacific Convergence Zone; second by investigating spatial variability of SMOS S_{1cm} related to rainfall. The resulting estimated S_{1cm} decrease associated with rainfall occurring within less than 1 h from the salinity measurement is close to −0.2 pss (mm h^{-1}) $^{-1}$. We estimate that rain induced roughness and atmospheric effects are responsible for no more than 20% of this value. We also study the signature of rainfall on sea surface salinity measured by surface drifters at 45 cm depth and find a decrease associated with rainfall of −0.21 (±0.14) pss (mm h^{-1}) $^{-1}$, consistent with SMOS observations. When averaged over one month, this rain associated salinity decrease is at most −0.2 in monthly 100 × 100 km^2 pixels, and at most 40% of the difference between SMOS S_{1cm} and interpolated in situ bulk salinity in pixels near the ITCZ. This suggests that more than half of this difference is related to the in situ products obtained from optimal interpolation and therefore influenced by smoothing and relaxation to climatology. Finally, further studies on the satellite-derived salinities should pay attention to that as well as to other sources of uncertainties in satellite measurements and not interpret fully the observed differences between in situ and satellite mapped products, as rain induced SSS variability.

1. Introduction

Several recent studies have concluded that climate change causes major changes in the global water cycle (see reviews in *Terray et al.* [2011] and *Rhein et al.* [2013]). Given that most of the evaporation and precipitations occur over the ocean, a main challenge for studying the global water cycle is the monitoring of freshwater fluxes over the ocean [*Schmitt*, 2008]. However monitoring these fluxes is difficult, in large part because precipitation is a very variable and intermittent process. Hence, it has been shown that the measure of sea surface salinity (SSS) provides an indirect but integrated information on air-sea freshwater flux that might be powerful for monitoring changes in the water cycle [*Gordon and Giulivi*, 2008; *Rhein et al.*, 2013]. This was one of the major motivations for observing SSS from space and two satellite salinity missions: the Soil Moisture and Ocean Salinity (SMOS) [*Kerr et al.*, 2010; *Font et al.*, 2010] and the Aquarius [*Lagerloef et al.*, 2008] missions, which now have provided global SSS fields over the last several years [e.g., *Reul et al.*, 2013; *Lagerloef*, 2012].

Using SSS as a rain gauge is however not trivial as it requires a precise estimation of other processes contributing to it, in particular ocean circulation processes often found to be on the same order of magnitude but opposite to the atmospheric flux [e.g., *Durand et al.*, 2013; *Hasson et al.*, 2014]. In the case of the satellite measurements, this is even more complicated by the fact that L-band radiometry senses the salinity in the first centimeter of the sea surface, S_{1cm}, which, under rainfall, may be much affected by surface stratification [e.g., *Soloviev and Lukas*, 1996; *Reverdin et al.*, 2012]. In addition, the accuracy of S_{1cm} measured by radiometry is expected to degrade in presence of rain due to imperfect knowledge of atmospheric rain effect, although the latter is expected to remain smaller than at higher frequency [*Wentz*, 2005], and to rain induced sea surface roughness [*Tang et al.*, 2013] which is very badly known. In both cases, this imperfect knowledge is also due to the difficulty of monitoring the rain characteristics (e.g., temporal and spatial distribution, droplet size, atmospheric profile).

Recent comparison between satellite S_{1cm} and salinity at a few meter depth, S_{bulk}, either measured in situ [*Boutin et al.*, 2013] or derived from the HYbrid Coordinate Ocean Model (HYCOM) model [*Tang et al.*, 2013]

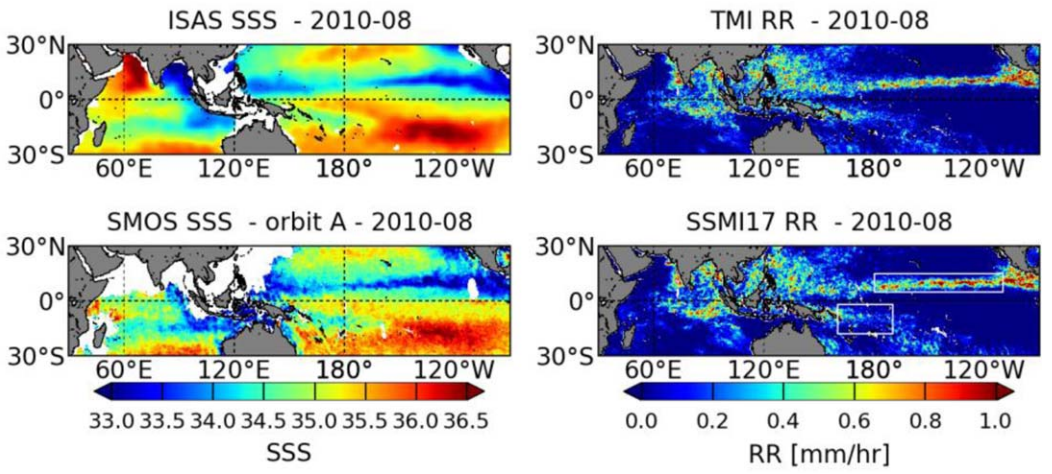

Figure 1. (left) SSS maps in August 2010 derived from (top) ARGO measurements using the ISAS version 6 D7CA2S0 optimal interpolation at 5 m depth [*Gaillard*, 2012]; (bottom) SMOS measurements during ascending orbits (6 AM) (LOCEAN CEC CATDS 2013 product); (right) Rain rates derived from (top) monthly TMI measurements; (bottom) monthly SSMI F16 measurements with superimposed white boxes that indicate the regions in which we study SMOS-ARGO SSS differences.

outline significant differences correlated with the presence of rain. The analysis of the Aquarius scatterometer indicates significant influence of rain on sea surface roughness, especially at low wind speed. The analysis of Aquarius radiometer brightness temperatures, Tb, indicates that in tropical regions vertical polarized Tb are often more affected by rain than horizontal polarized Tb. This suggests that the radiometric signal is often more affected by surface dilution process than by roughness effect, although this is not the case at high latitudes [*Tang et al.*, 2013]. Nevertheless, this analysis uses modeled atmospheric wind speed (NCEP) which validity in local rain cells is difficult to assess and HYCOM simulated SSS which represents a bulk salinity at a few meters depth. Actually, in most cases there is no matchup between L-band radiometer measurement in a rain cell and either ground truth SSS measured in the first top centimeters or a roughness related parameter (e.g., wind speed) while SSS vary a lot in rainy regions. Indeed, *Boutin et al.* [2013] showed on a particular example that ARGO S_{bulk} taken under rainy conditions may be 0.7 fresher than ARGO S_{bulk} measured 10 days later in non rainy conditions, i.e., that rain induces a large and rapid variability on ARGO S_{bulk}, while we could not find SMOS S_{1cm} data within a few hours from rainy ARGO S_{bulk}, thus preventing a direct comparison between S_{1cm} and S_{bulk}, under rainy conditions.

We will investigate the robustness of the relationship found in *Boutin et al.* [2013] between SMOS S_{1cm} minus ARGO S_{bulk} and rain rate. We will also investigate the spatial variability of SMOS S_{1cm} in and around rain cells, and the impact of the undersampling of this variability by ARGO floats which measure salinity deeper than SMOS, at about 5 m depth, and which spatial and temporal coverage is much more sparse than the one of SMOS. We will focus on rainy regions such as the Intertropical Convergence Zone (ITCZ) and the Southern Pacific Convergence Zone (SPCZ) where large scale differences are observed between SSS maps derived from SMOS S_{1cm} and from ARGO S_{bulk} (Figure 1).

For that, we extend the analysis of SMOS S_{1cm}-ARGO S_{bulk} in rain cells done in the ITCZ [*Boutin et al.*, 2013] to longer periods as well as to the SPCZ. In addition, we study the spatial variability of SMOS S_{1cm} associated with rain and compare its magnitude with SSS variability observed in situ at about 45 cm depth, $S_{45cm,}$ by surface drifters. Data and Methods are detailed in section 2, Results are presented in section 3 and discussed in section 4.

2. Data and Methods

2.1. SMOS

The SMOS mission [*Kerr et al.*, 2010] has been launched in November 2009, on a sun-synchronous circular orbit with a local equator crossing time at 6 AM on ascending node. It carries a L-band interferometric radiometer. This new technology allows reconstructing bidimensional multiangular images of Tb with a mean

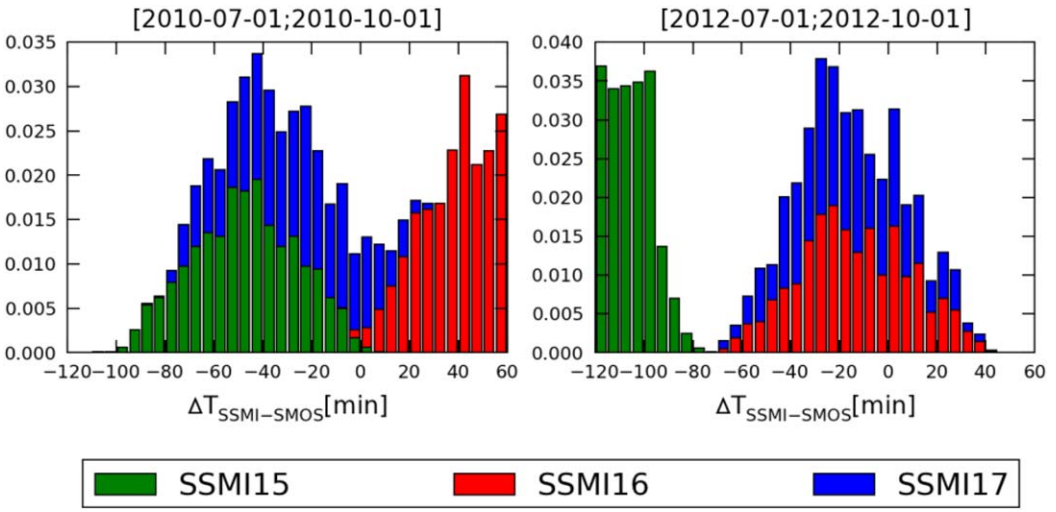

Figure 2. Histogram of the time difference between SMOS and SSM/I colocated measurements in ITCZ region (green: SSM/I F15; red: SSM/I F16; blue: SSMI F17). (left) July–September 2010; (right) July–September 2012.

spatial resolution of 43 km. Individual measurements are very noisy (the typical noise on individual retrieved S_{1cm} is 0.6 in tropical and subtropical regions, as derived from comparisons with ARGO measurements [*Boutin et al*., 2012, Figure 6] or estimated by the retrieved algorithm [*Hernandez et al*., 2014, Figure 2a]; however this noise can be reduced by averaging S_{1cm} in space and time [*Boutin et al*., 2004]. The retrieval scheme implemented in the ESA (European Space Agency) processing retrieves SMOS S_{1cm}, wind speed, sea surface temperature (SST), total electron content, and their theoretical errors, from the multiangular and polarized SMOS Tbs collected at an earth pixel during the satellite pass, using Levenberg-Marquard (L.M.) minimization method as described in [*Zine et al*., 2008]. Prior values for wind speed and SST are taken from European Centre for Medium-Range Weather Forecasts (ECMWF); in the ESA operational chain, errors of 2 m s^{-1} and of 1°C have been attributed to wind components and SST respectively. The theoretical errors are retrieved from the Jacobian of Tb with respect to the geophysical parameters and from the a posteriori covariance matrix of errors in Tb and geophysical parameters [see *Zine et al*., 2008]. At first order, the theoretical error of S_{1cm} depends on the number of Tb data used in the retrieval and on SST (because of the strong dependency of dTb/dSSS with SST).

In the present study, we use the level 2 SMOS S_{1cm} from the first SMOS/ESA annual reprocessing campaign in which ESA level 1 v5.04 and level 2 v5.50 processors have been used (see a complete description in the Algorithm Theoretical Basis Document (ATBD) available on http://www.argans.co.uk/smos/docs/deliverables/delivered/ATBD/SO-TN-ARG-GS-0007_L2OS-ATBD_v3.8_111117.pdf). Large scale seasonal biases, likely due to flaws of the thermal antenna model [*Kainulainen et al*., 2012] are still present in this version. In the southern tropical Pacific Ocean, they are corrected by the application of the Ocean Target Transformation so that the rms error of monthly – 100 × 100 km^2 SMOS S_{1cm} with respect to ship S_{bulk} has been found equal to 0.20 in the south east Pacific between 0° and 30°S, a region with very few rain events [*Hasson et al*., 2013]. On another hand, *Hernandez et al*. [2014] have shown large biases (several tenths of pss) in the northern subtropical Atlantic region (15°N–35°N), largest in boreal winter. Once these large scale monthly biases are removed, the rmse of monthly – 100 × 100 km^2 SMOS S_{1cm} with respect to ship measurements is equal to 0.15. We have chosen the boreal Summer season for collocating SMOS SSS with ARGO SSS in the ITCZ (Intertropical Convergence Zone) because it corresponds to a period of relatively low biases north of the equator as found in the North Atlantic subtropical regions [*Boutin et al*., 2013]. Hence in the present study, we extend the SMOS S_{1cm}-ARGO S_{bulk} comparison in the ITCZ region to boreal summers 2010 and 2012; a much longer period (June 2010 to February 2011) is considered for the SMOS-ARGO comparison in the SPCZ (south of the equator) for which the OTT is assumed to correct for seasonal biases.

We use ESA level 2 SMOS S_{1cm} retrieved with model 1, which makes use of the [*Yin et al*., 2012b] roughness model; only ascending orbits are considered in order to minimize uncertainties linked to Faraday rotation and to diurnal SST cycle.

The filtering of the ESA level 2 SMOS S_{1cm} is performed as follows: we retain grid points flagged as valid, as well as with successful retrieval, with a good fit between measured and modeled Tbs (tests on Chi2 and Chi2_P as defined in ATBD), with less than 20 iterations of the Levenberg and Marquardt retrieval process, with no suspicious ice or numerous outliers. In addition, in order to 1) avoid too noisy retrievals at the edge of the swath and 2) inaccuracy due to lower accuracy of ECMWF forecasts or of the roughness model at very low and high wind speed, we only consider SMOS S_{1cm} retrieved in grid points with 1) more than 130 Tb coming from the alias free field of view region (roughly corresponding to S_{1cm} retrieved at $\pm$300 km from the centre of the track) and 2) ECMWF wind speed between 3 and 12 m/s. The averages of ESA level 2 SMOS S_{1cm} are weighted with theoretical error and measurement resolution as described in [*Yin et al*., 2012a]. Only averages made with more than 30 individual SSS are retained. With these criteria, a grid point is seen approximately once every 5 days, during ascending orbits.

2.1.1. Two Step Retrieval Algorithm

Yin et al. [2013] have shown that in cases when ECMWF wind speed differs from SSM/I radiometric wind speed, the SMOS retrieval scheme corrects part of the difference between these two wind speeds and this improves the quality of the retrieved S_{1cm}. In cases of large differences between these two wind speeds, they tested a SMOS retrieval with a larger a priori error on wind speed (5 m s^{-1} instead of 2 m s^{-1}). This resulted in a retrieved wind speed closer to SSM/I, a smaller bias on SSS, but also increased noise on retrieved parameters. In order to correct biases without increasing too much the noise, we have developed an alternative retrieval algorithm (two step algorithm). In a first step, the error on a priori ECWMF wind speed is set to 5 m s^{-1}. This results in a very noisy retrieved wind speed over the 15 km resolution ISEA grid which is then filtered using a bidimentional spatial median filtering having a 50 km radius. In a second step, the smoothed retrieved wind speed is used as a priori wind speed (instead of ECMWF) with an error set to be 2 m s^{-1}. This method has been successfully tested in the eastern equatorial Pacific region (5°S–1°N; 90°W–130°W) in August 2010 where a systematic bias is observed on both SMOS retrieved S_{1cm} (a 0.46 difference with respect to ARGO S_{bulk}) and on ECMWF wind speed (1.4 m s^{-1} difference with respect to radiometric SSM/I wind speed), although the operational method already corrects for half of the ECMWF minus SSM/I wind speed difference [*Yin et al*., 2013]. When applying the two step retrieval method instead of the operational retrieval method, the SMOS S_{1cm} bias with respect to ARGO S_{bulk} is reduced from 0.46 to 0.26, and the SMOS retrieved wind speed is decreased by 0.4 m s^{-1} making it very close (0.3 m s^{-1} difference) to the wind speed retrieved when using SSM/I wind speed as the guess instead of ECMWF wind speed (*Yin et al*., poster at the ESA Living Planet Symposium, http://www.argans.co.uk/smos/pages/posters.php?poster=LPS2013_Yinetal.pdf).

Rain splash modifies the ocean roughness as seen by the radiometer, which should be affecting more Th than Tv at large incidence angle contrary to what is induced by a change in S_{1cm}. Hence, given that SMOS retrieval uses the polarized Tb at various incidence angles to separate SSS and roughness (parametrized in terms of wind speed) signals, one expects the retrieved wind speed to be modified by a change in rain induced roughness. In order to test the importance of this change for rainy SMOS measurements, we have looked at S_{1cm} retrieved with the two step algorithm.

2.1.2. Natural Variability of SMOS SSS

Individual SMOS SSS are very noisy. In order to distinguish between the expected noise due to the radiometric noise and the variability due to other effects, we compute the quadratic difference between the standard deviation of SMOS SSS within one month and 100 x 100km^2 and the theoretical error averaged over the same time and spatial scales using weights depending on the SMOS measurements resolution and on the theoretical errors [see *Yin et al*., 2012a, equation (A8)]. Assuming that the theoretical error provided with retrieved SMOS SSS is a realistic estimate that takes into account all error sources, this computation represents the natural variability in one month of S_{1cm} averaged over 43 km, as in SMOS.

2.2. Satellite Rain Rate and Wind Speed

Satellite rain rates (RR) and wind speeds from WindSat version 7.0.1, SSM/Is F15, F16 and F17 version 7, AMSR-E and TMI version 4, distributed by Remote Sensing System (www.remss.com) have been used. They were derived from the Unified Microwave Ocean Retrieval Algorithm (UMORA) described in [*Hilburn and Wentz*, 2008] after thorough intercalibration of the SSM/Is data as described in *Wentz* [2013]. SSMI F15 quality degrades after August 2006 and RemSS recommend not to use it for climate studies. Nevertheless, we

Table 1. SMOS Minus ARGO SSS Versus SSM/I Rain Rate Obtained With Two Time Colocation Radii[a]

	aRR+b	r	N
Zone ITCZ (Jul–Sep 2010)			
Ssmos-Sargo (−60 min;+30 min)	−0.18(0.007)RR-0.16	−0.49	9705
Ssmos-Sargo (−30 min;+15 min)	−0.18(0.011)RR-0.14	−0.43	4453
Ssmos_twostep-Sargo(−60 min;+30 min)	−0.17(0.007)RR-0.11	−0.45	9704
Ssmos_twostep-Sargo(−30 min;+15 min)	−0.16(0.011)RR-0.09	−0.39	4458
Zone SPCZ (10 Jun to 11 Feb)			
Ssmos-Sargo (−60 min;+30 min)	−0.21 (0.012) RR-0.23	−0.49	3691
Ssmos-Sargo (−30 min;+15 min)	−0.17 (0.019) RR-0.17	−0.38	1697
Zone ITCZ (Jul–Sep 2012)			
Ssmos-Sargo (−60 min;+30 min)	−0.22 (0.007)RR-0.18	−0.56	7915
Ssmos-Sargo (−30 min;+15 min)	−0.22 (0.008)RR-0.17	−0.58	5694

[a](−60 min;+30 min) and (−30 min;+15 min)

consider it in our RR colocations as we are not performing climate studies but we are considering large instantaneous RR variability for which SSM/I F15 can be very complementary to the other satellite measuring RR. For most SSM/I missions, the local equator crossing time is close to 6 PM, although for some of them (in particular SSM/I F15), it drifts in time (see http://www.remss.com/support/crossing-times). As a consequence, the closest colocations between SMOS and satellite RR are found with SSM/I. In July–September 2010, the period during which the analysis of the SMOS S_{1cm}-ARGO S_{bulk} differences was the most extensive, the majority of SSM/I measurements were at more than 3 0min from SMOS measurements, although by less than 1:30 (Figure 2, left). Nevertheless, given the SSM/I time drift, in July–September 2012, the majority of SSM/I F16 and SSM/I F17 were closer to SMOS measurements, within (−30 min; +15min). As a consequence, we consider two time intervals in our SMOS-SSM/I matchups: (−60 min; +30 min) and (−30 min; +15 min); only the satellite RR closest in time with SMOS SSS is retained.

In addition to individual satellite RR products, in order to get information about RR whatever the local time is, we use the TRMM3B42 product version 7 (http://disc.sci.gsfc.nasa.gov/precipitation/documentation/TRMM_README/TRMM_3B42_readme.shtml) which provides RR estimate over 3 hours. It is used to distinguish between ARGO SSS measured under rainy or non rainy conditions. However, the 3 h time resolution is insufficient to characterize the correlation between SMOS S_{1cm} – ARGO S_{bulk} and RR: using the TRM3B42 RR product instead of SSM/I RR colocated within (−60 min;+30 min) degrades the correlation coefficients (as reported in Table 1) by a factor 1.4–1.6.

2.3. ARGO SSS

We use measurements from ARGO floats provided by the Coriolis data centre (http://www.coriolis.eu.org/), with a quality flag equal to 1, in agreement with real time quality checks and, for delayed time data, with statistical consistency checks [*Carval et al.*, 2012]. In order to avoid unpumped measurements [see *Boutin et al.*, 2013] we use the closest ARGO salinity to the sea surface, provided it is measured between 4 m and 10 m depth, without any interpolation to the surface. We will later refer to this measurement as ARGO S_{bulk}. These ARGO S_{bulk} are colocated with SMOS S_{1cm} within a radius of ±5 days and ±50 km. Contrary to what was done in [*Boutin et al.*, 2013] in which we colocated all ARGO S_{bulk} with SMOS S_{1cm} whatever the rain conditions were at the time of ARGO measurement, in the present study we exclude rainy ARGO S_{bulk} identified by TRMM3B42 product within −2 h and +1 h from each ARGO measurement. This test identifies that 24% of the ARGO measurements have occured at less than 2 hours from a rain event in the ITCZ region. The ARGO S_{bulk} taken under rainy conditions are discarded from the SMOS S_{1cm} – ARGO S_{bulk}. Thus, S_{1cm} minus S_{bulk} will represent an upper bound of the vertical stratification effect.

2.4. SVP Drifters

A large set of Surface Velocity Drifters (SVP) measuring conductivity and temperature at about 45 cm depth have been deployed for the new salinity satellite calibration and validation. They have been thoroughly quality checked [*Reverdin et al.*, 2014]. They show large salinity variability often associated with rainfall [*Reverdin et al.*, 2012]. Hence we develop a method that automatically detects sharp and local decrease of SSS, SSS_{min}, possibly affected by rain. A S_{45cm_min} is identified as affected by rainfall if:

1. the difference between the median of the S_{45cm} measured every 30 min during the 6 h preceding S_{45cm_min} (S_{45cm_ref}) and S_{45cm_min} is larger than 0.4,
2. the difference between the median of the S_{45cm} measured every 30 min during the 6 hours after S_{45cm_min} and S_{45cm_min} is larger than 0.2,

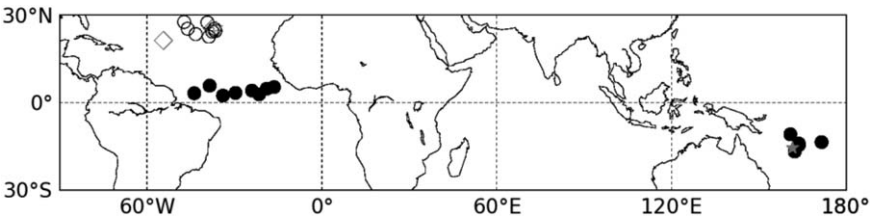

Figure 3. Locations of S_{45cm} large decreases measured by drifters and colocated with RR. The black filled and open circles are for moderate (3–12 m s^{-1}) wind speed conditions in respectively tropical and subtropical regions; the gray losanges are for low wind speed (<3 m s^{-1}), the gray stars are for high wind speeds (>15 m s^{-1}).

3. S_{45cm_min} is a local minimum : at least 0.02 smaller than S_{45cm} measured just before and just after S_{45cm_min} and S_{45cm} measured every half hour during the 2.5 h after S_{45cm_min} must increase by at least 0.01 per 0.5 h, in order to avoid misidentifying crossing of fronts as rainfall events.

Using this test, 470 events of sharp and large S_{45cm} decrease events have been identified since 2009. This number was not sufficient to obtain reliable comparisons between drifters and SMOS S_{1cm} under rainy conditions, especially since such colocations must be done within a small temporal radius and because the large noise on SMOS S_{1cm} requires to average a large number of measurements to get statistically significant results.

Hence, instead of a direct comparison of drifter S_{45cm} with SMOS S_{1cm} under rain cells, we compare the SSS decrease associated with satellite rain rate either deduced from SMOS S_{1cm} or from drifters S_{45cm}.

2.5. SMOS SSS Decrease Associated With Rain Rates

Two methods have been tested to estimate the SMOS S_{1cm} decrease under rain cells. The first method, similar to the one used in [*Boutin et al*., 2013], is based on differences between SMOS S_{1cm} and ARGO S_{bulk} by taking SMOS S_{1cm} at ±50 km and ±5 days from ARGO floats. Given the intermittency of rain, we do not average SMOS measurements. Instead, the SMOS S_{1cm}-ARGO S_{bulk} differences are analyzed as a function of the SSM/I satellite rain rate acquired the closest in time to the SMOS SSS measurement within an interval of either −60 min and +30 min, or −30 min and +15 min. This method was applied in the ITCZ (5°N–15°N; 180°W–110°W) as in [*Boutin et al*., 2013], and in the SPCZ (18°S–2°S; 160°E–170°W). As mentioned earlier, the ITCZ study is done in boreal summer to minimize SMOS large scale biases effects. On the other hand, since large scale biases are expected to be small in the latitudinal range of the SPCZ region and given the smaller size of the chosen "SPCZ" region, we extend the studied period to June 2010 to March 2011 in order to get a more significant number of SMOS/ARGO-RR colocations.

The second method, independent of any in situ SSS comparison, correlates the spatial variability of SMOS S_{1cm} with the one in RR maps.

Spatial variability of SMOS S_{1cm} associated with the presence of rain cell has been determined from a comparison with a spatial field of satellite RR taken as close as possible in time from the SMOS SSS field (at typically less than half an hour), as follows. First, we identify, over a given region, the SMOS pixels located at less than 100 km from a pixel with a satellite RR larger than 5mm h^{-1}. For each of these rainy SMOS S_{1cm} pixels, we estimate the rain effect on S_{1cm} as the difference between the local SMOS S_{1cm} and an estimated "rain-free" S_{1cm} taken as the mean of the S_{1cm} colocated with a null RR within less than 150 km from the local SMOS S_{1cm}.

2.6. Drifters and RR Colocations

Amongst the 470 sharp S_{45cm} decreases observed by drifters and identified as described in section II.4, 24 have been colocated with satellite RR passes at less than ±15 min (see their location in Figure 3); the ±15 min temporal radius corresponds to half the interval between successive drifter S_{45cm} measurements while a huge variability is observed on successive drifter S_{45cm} around the S_{45cm} minimum, likely due to the temporal variability of precipitation. The magnitude of the S_{45cm} decrease, DSSS, has been estimated as S_{45cm_min}-S_{45cm_ref} (see section 2.4) in most cases (see an example on Figure 4, top), except if the decrease appears to be discontinuous: in that case S_{45cm_ref} is taken equal to the local maximum preceding S_{45cm_min} (see an example on Figure 4, middle). We associate DSSS with the average of the rain rates in 0.25° pixels which centers are at less than 50 km from the drifter location at the time of DSSS; this corresponds approximately to averaging RR measured in the pixel containing the drifters, and in the ones adjacent to it. We do

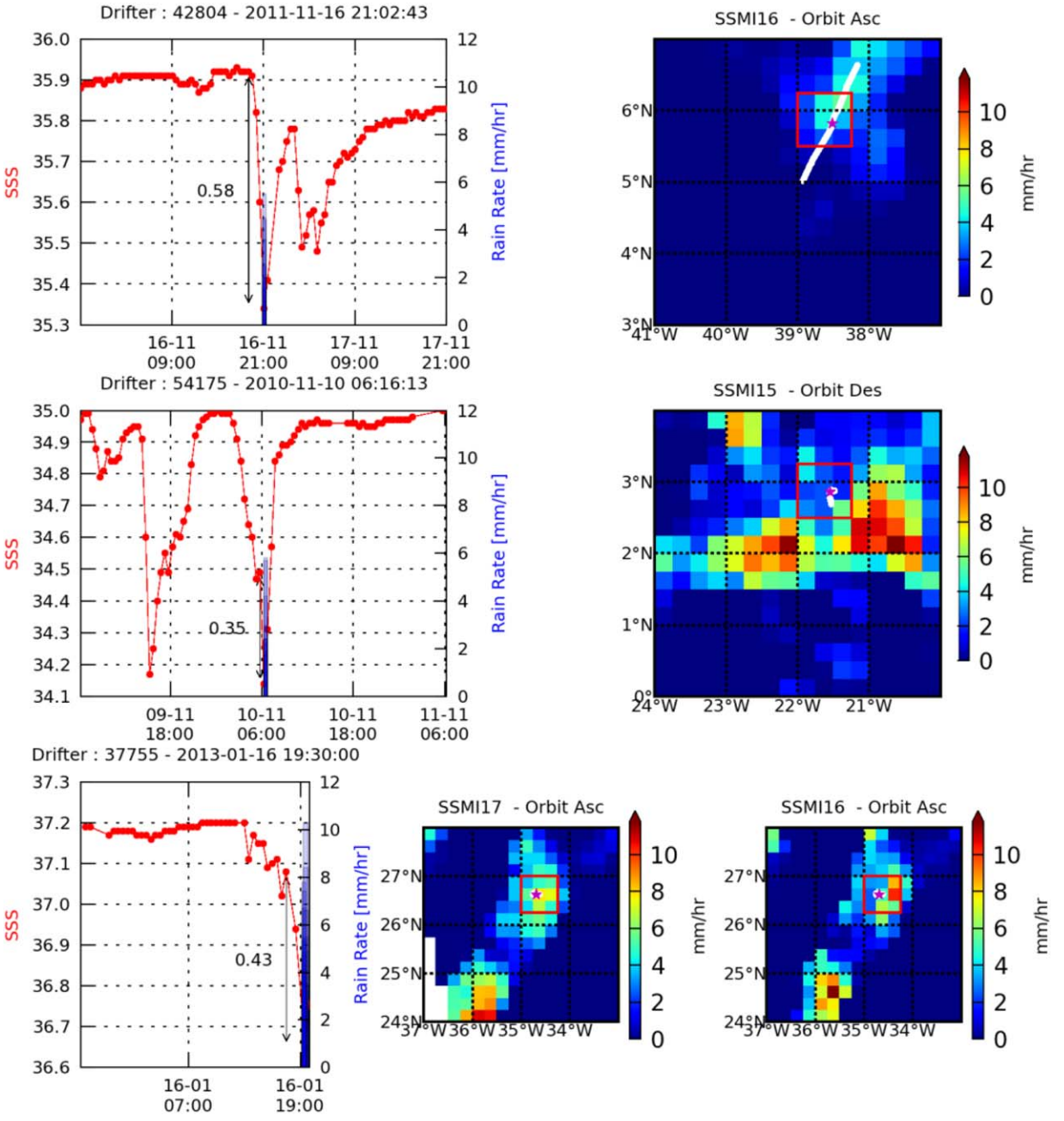

Figure 4. Time series of drifter SSS just before and after SSS_{min} (left column) and associated maps of RR with superimposed drifter trajectory (white; ±24 h around the SSS minimum); violet point corresponds to drifter position when SSS is minimum (right). The RR values in adjacent pixels around the sharp SSS decrease observed by the drifter are plotted as blue bars on figure left. Top: example of a continuous decrease; middle: example of a discontinuous decrease; (bottom) example of a rain event sampled by SSMI F17 6 min before the S minimum measured by the drifter and by SSMI F16 6 min after, illustrating the large variability of RR within less than 15 min.

not only consider RR in the pixel containing the drifter in order to smooth the large temporal variability of rain within 15 min; actually successive SSM/I maps, at less than 15 min interval, show a huge temporal variability (see Figure 4, bottom); when smoothing this variability over 9 RR pixels, it is much reduced.

It is very difficult to get information about wind speed under rain cells. Actually most of satellite wind speeds are flagged under rain conditions; an "All Weather" [*Meissner and Wentz*, 2009] product containing a wind speed under rain cells is provided only with WindSat, while only 3 matchups have been found with WindSat. Hence, for the other matchups, we very crudely estimate a range of wind speed from a visual inspection of

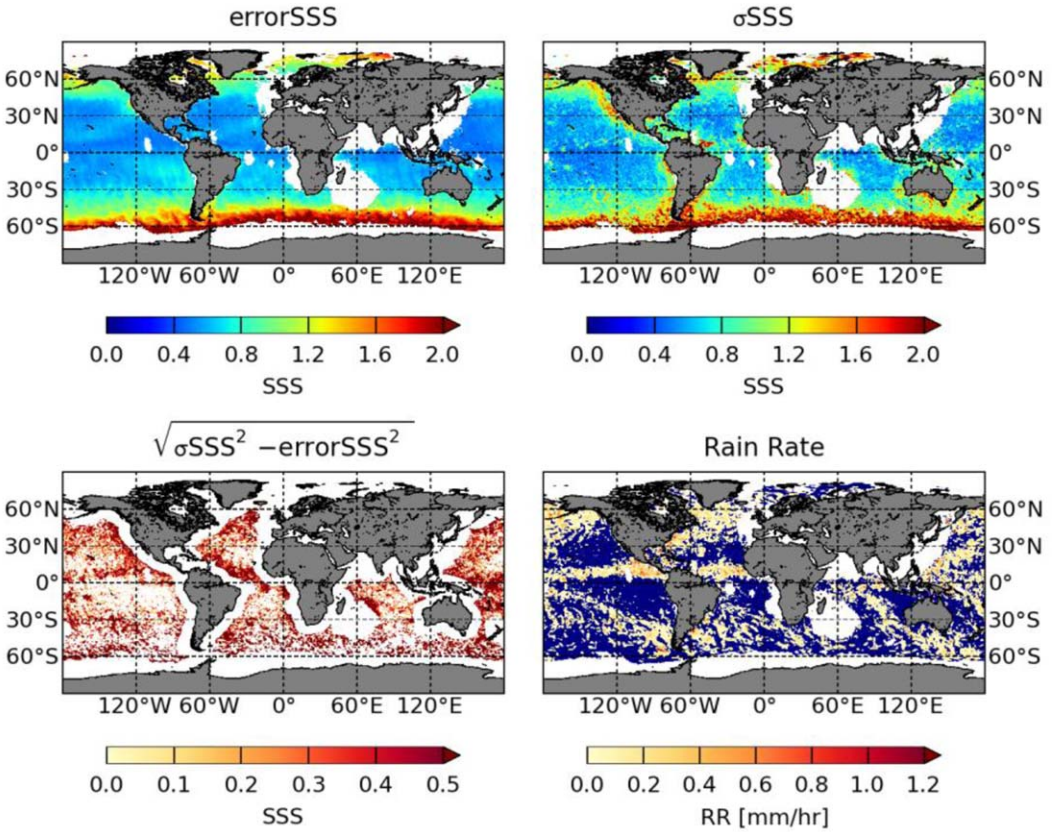

Figure 5. (top left) Mean theoretical error; (top, right) monthly SSS standard deviation; Bottom left : SSS variability observed by SMOS when mean theoretical error has been removed (pixels at less than 800 km from large land masses in which SMOS image reconstruction is imperfect have been removed); (bottom right) Satellite rain rate. All figures are from August 2010.

the radiometric wind speed maps around the rain cell. We classify our matchups in three categories, very low wind speed (less than 3 m s^{-1}), moderate wind speed (3–12 m s^{-1}) and strong wind speed (larger than 15 m s^{-1}; there were no matchups corresponding to a wind speed between 12 and 15 m s^{-1}).

3. Results

The observed variability of SMOS S_{1cm} (Figure 5, top right) is large, but in general it is close to the one expected from the radiometric noise (Figure 5, top left). This is not the case (Figure 5, bottom) 1) in the vicinity of large land masses likely due to imperfections in SMOS image reconstruction and to large natural S_{1cm} variability in coastal areas, and, 2) in rainy regions possibly due to large natural variability on S_{1cm} induced by rain or to rain induced radiometric variability not related to salinity (e.g., imperfect correction of atmospheric/roughness effect). When taking the quadratic mean of the observed minus expected variability (Figure 5, bottom left), within the ITCZ region, we estimate that rain could induce a mean S_{1cm} variability of 0.33.

When SMOS S_{1cm} are colocated with ARGO S_{bulk}, similar trends are observed between SMOS S_{1cm}-ARGO S_{bulk} and SSM/I rain rate (slope close to -0.2 pss (mm h^{-1}) $^{-1}$) in ITCZ and SPCZ (Table 1). The slope in the ITCZ region in 2010 (-0.18 pss (mm h^{-1}) $^{-1}$) (Figure 6, left) is slightly smaller than the one reported in *Boutin et al.* [2013] (-0.16 pss (mm h^{-1}) $^{-1}$) because we have eliminated ARGO S_{bulk} acquired in presence of rain. In 2012, in the ITCZ (Figure 6, right), when the SSM/I measurements were closer in time with the SMOS ones, the correlation coefficients increase and the slope slightly decreases to -0.22 pss (mm h^{-1}) $^{-1}$. All the colocations results shown in Table 1 indicate a decrease of SMOS S_{1cm} within less than one hour from a rainfall event of about -0.2 pss (mm h^{-1}) $^{-1}$.

When the SMOS S_{1cm} in the ITCZ is retrieved with the two step algorithm instead of the operational algorithm, the slope of the fit (in absolute value) is very slightly decreased (Figure 6, left), and this decrease is at the limit of the significance. Hence a rain-roughness effect is likely to occur but is a second order effect (less than -0.013 pss (mm h^{-1}) $^{-1}$, i.e., less than 8% of the total rain effect) with respect to the SSS decrease.

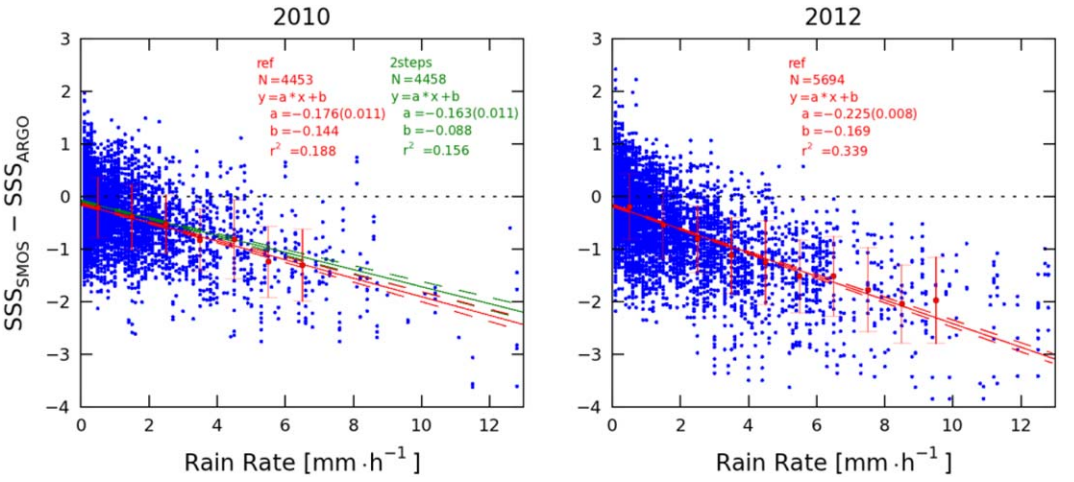

Figure 6. SMOS minus ARGO S versus SSM/I rain rate colocated within (−30 min;+15 min) in ITCZ region. (left) July–September 2010; (right) July–September 2012. The blue points correspond to individual SMOS SSS retrieved with the default algorithm. The red dots and bars indicate the mean plus and minus 1 standard deviation of SSSsmos-SSSargo within 1 mm/h RR classes provided classes contain more than 30 SMOS SSS. The corresponding fit (plain line) and its 95% confidence interval (dashed line) is plotted in red. On figure left, we have also superimposed the fit and 95% confidence interval obtained from SMOS SSS retrieved with the two step algorithm (green).

The spatial variability of SMOS SSS observed close to rain cells is very well correlated with rain rates, provided that the temporal lag between the SMOS SSS and the satellite RR is short. An example taken in the northern subtropical Atlantic region is shown on Figure 7. In this particular case, the correlation between DSSS and RR taken by SSMI F17 (Figure 7, right) at less than half an hour interval is quite good (r=−0.67). In this particular case, the effect of rain on SMOS retrieved SSS is −0.18 (±0.019) pss (mm h^{-1}) $^{-1}$. On the other hand, the correlation with the SSMI F15 RR taken 1 h30 before the SMOS pass (Figure 7, left) is much less (r=−0.48). We could not identify any spatial structure in DSSS similar to the one of rain rate sampled by SSMI F15. Hence the influence of the rain history on this particular example could not be ientified. This is likely because this example was taken under moderate wind speed (SSM/I wind speed near the rain event was on the order of 9 m s^{-1}).

When considering the S_{45cm} decrease measured by the drifters and collocated with the satellite rain rate, we observe quite a large scatter (Figure 8). Two outliers with low DSSS and large RR have been identified as

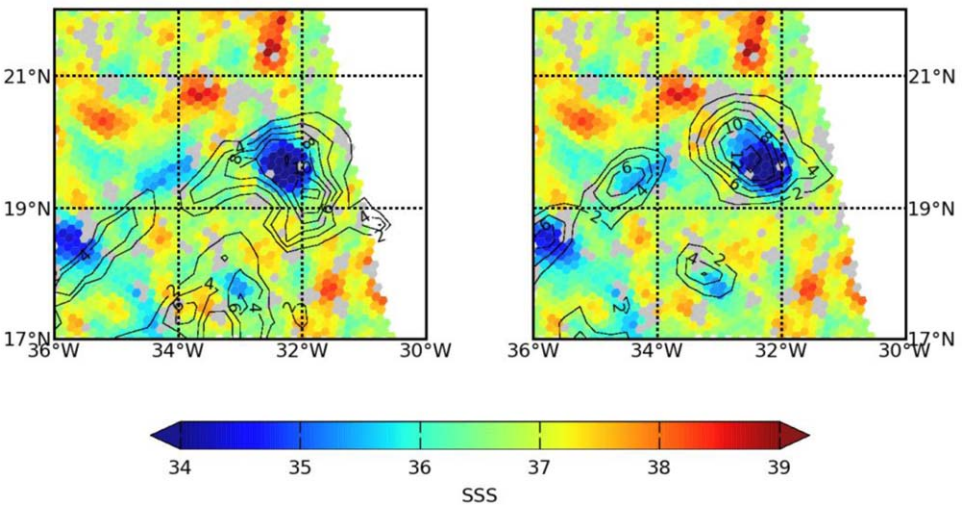

Figure 7. SMOS SSS (color) and satellite rain rate (isolines from 2 to 12 mm/h) on 26 August 2012. SMOS pass was on 8:02 TU and satellite rain rate passes left) from SSMI F15 on 6:18 TU and right) from SSMI F17 on 8:30 TU. SSM/I wind speed measured in the vicinity of this rain event was about 9 m s^{-1}.

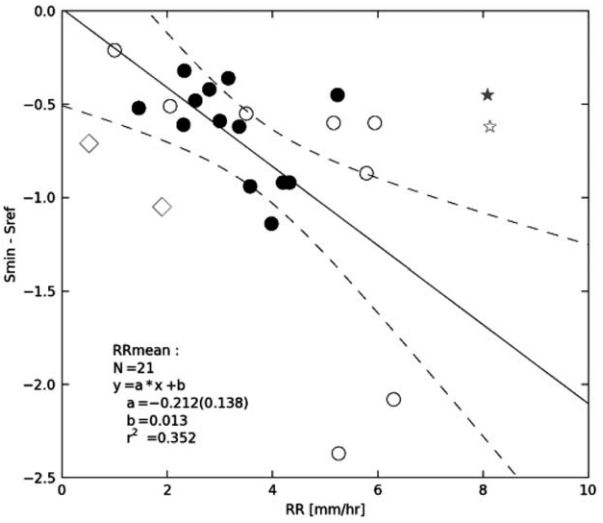

Figure 8. DSSS versus RR. Filled dots: tropical region; Open dots: subtropical region. The black filled and open circles correspond to moderate wind speed (3–12 m/s); the gray losanges correspond to low wind speed (<3 m/s), the gray stars correspond to high wind speeds (>15 m/s). The linear regression and the associated 95% confidence interval obtained for moderate wind speed conditions are represented with a continuous line and with dashed lines respectively.

corresponding to high wind speed (>15 m s^{-1}), in which case mixing is expected to much reduce the surface freshening. Two outliers with relatively large DSSS and small RR have been identified as occurring in regions of low wind speed (<3 m s^{-1}). The rest of the points have been acquired with moderate wind speed (between 3 and 12 m s^{-1}) When these four outliers are removed, the slope of the fit computed over 21 points is −0.21 (±0.14) pss (mm h^{-1}) $^{-1}$.

We then test removing this rain related effect (∼−0.2 pss (mm h^{-1}) $^{-1}$) onto one month of SMOS S_{1cm} and satellite RR. This correction is expected to suppress local large decrease of S_{1cm} concommittent with rain events. On average over one month, this correction is locally at most 40% of the difference between SMOS S_{1cm} and interpolated ARGO S_{bulk} mapped products (Figure 9). A correction of −0.2 pss (mm h^{-1}) $^{-1}$ only very slightly reduces the "natural" variability derived from SMOS measurements (not shown; uncorrected variability shown on Figure 5, bottom left) : the quadratic mean of this "natural" variability in the ITCZ becomes 0.31 after rain induced variability removal (it was 0.33 before correction). We compare this estimate with the variability

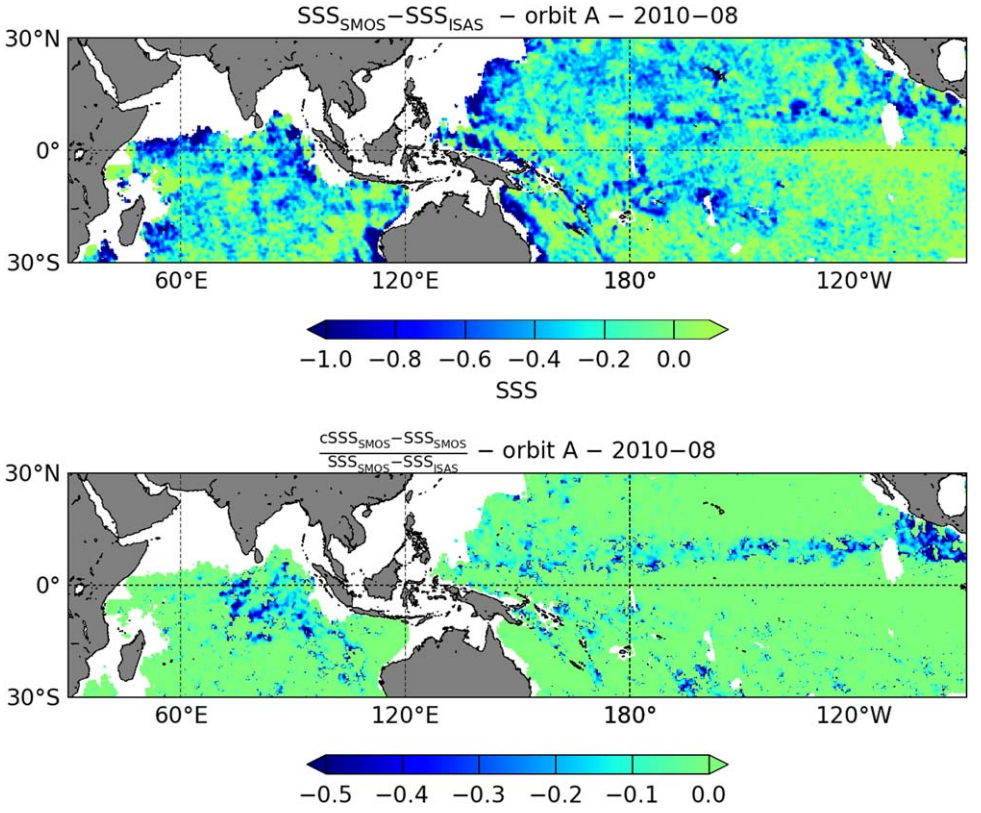

Figure 9. (top) SMOS minus ARGO interpolated salinities shown on Figure 1; (bottom) ratio between the rain induced salinity decrease and the SMOS minus ARGO interpolated salinities.

of individual ARGO S_{bulk} as compared to ARGO interpolated monthly S_{bulk}. The standard deviation of the difference between individual ARGO S_{bulk} and monthly S_{bulk} in interpolated maps is 0.24, both with or without eliminating ARGO measurements obtained less than 2 h from rain events.

4. Discussion and Conclusion

We estimate the local effect of rain on decreasing SMOS S_{1cm} with two approaches. First, we compare S_{1cm} in a rain cell with S_{1cm} acquired in its vicinity but outside the rain cell. This method quantifies the local spatial variability of S_{1cm}, within 30 min from a rain event. Secondly, we compare SMOS S_{1cm} with S_{bulk} measured by ARGO with no rain event close in time to the ARGO measurement. This is to prevent any influence of rainfall on ARGO S_{bulk} short-term variability which is expected to be very different from the one on SMOS S_{1cm} as the two measurements are not at the same depth and are always separated by at least several hours (up to ± 5 days). Hence, the SMOS minus ARGO SSS differences shown in this paper quantify the high variability of SSS_{1cm} associated to rain, that is expected to originate from both the intermittency of rain and the vertical stratification. From both approaches, the local signature of rain occurring within less than one hour from the SMOS S_{1cm} is between -0.18 and -0.22 pss (mm h^{-1}) $^{-1}$ depending on the region and on the method used to quantify the effect. It is also likely that the decrease in S_{1cm} is affected by the rain accumulated over several hours. However, on the example shown on Figure 7, corresponding to moderate wind speed (on the order of 9 m $s^{-1)}$, the impact of rain occuring 90 min before the SMOS pass remains unclear. We could not investigate further the influence of the rain history on SMOS minus ARGO colocations as there are very few cases when SMOS SSS is colocated with several satellite RR taken at a few hours interval which would have allowed to follow the rain history. We tried to consider the rain history effect on SMOS minus ARGO comparisons by using TRM3B42 product but the correlations were very poor, likely due to the 3 h resolution of the product. Future studies should probably focus on the influence of rain history for example by using precipitation analyses at higher spatial and temporal resolution.

This estimate is not corrected for the roughness changes in presence of rain; using less relaxation to ECMWF wind speed, we find that the roughness effect is at the limit of detection by SMOS and could decrease the effect by only 0.01 pss (mm h^{-1}) $^{-1}$. The neglected atmospheric contribution of rain to S_{1cm} retrieval is also expected to be small. It would be on the order of 0.03 pss (mm h^{-1}) $^{-1}$ based on a Rayleigh approximation [e.g., *Peichl et al.*, 2004; *Wentz*, 2005]. Hence, combining the contribution of these two effects, SMOS measurements suggest that the salinity decrease induced by rainfall in the first centimeter of the surface ocean is at least -0.14 pss (mm h^{-1}) $^{-1}$ at moderate wind speed (3–12 m/s). Given the present network of in situ salinity measurements, we could not find SMOS passes simultaneous to a rain event sampled at the same time by in situ instrument so that it is not possible to estimate the decrease with precise matchups between satellite and in situ measurements, nor to estimate directly the part of the variability originating from vertical stratification.

An attempt was made to check whether the order of magnitude of the SMOS S_{1cm} decrease is compatible with in situ S_{45cm}. Using matchups between S_{45cm} decreases measured by in situ drifters and satellite RR at less than 15 min from the drifter measurement and smoothed over $\sim$75 km, we find a rain signature of -0.2 pss (mm h^{-1}) $^{-1}$ ($r=-0.6$, thus a large uncertainty). If instead of taking smoothed RR, we consider RR in the closest pixel to the drifter, the slope of the fit becomes non significant. Similarly, if we consider matchups within 1 h instead of 15 min the slope becomes non significant. Nevertheless, in all these cases the ratio between the mean S_{45cm} drawdown (DSSS) and the mean RR averaged over the 21 rain events under moderate wind speed, remains equal to -0.2. Part of the scatter we observe in Figure 8 is due to the temporal sampling of the drifters (one measure every 30 min) and to the fact that it is a local measurement whereas RR is spatially integrated; nevertheless the S_{45cm} provides a temporal integrated information of the rain effect while the rain itself is very intermittent. Comparing local S_{45cm} measured by drifters with SMOS S_{1cm} integrated over 43 km is challenging but by averaging several drifter events, we expect to minimize the effect of spatial variability. On the other hand, rain events observed by drifters have been identified from S_{45cm} decrease larger than 0.4 so that in our analysis S_{45cm} decreases less than 0.4 associated with rain events have been neglected. Hence the mean S_{45cm} decrease associated with rain rate that we have estimated may be slightly overestimated.

The method for determining the SSS decrease is tricky as we do not normalize it by the duration of the decrease and we do not consider the accumulation of rain. This was not possible because high resolution rain history previous, during and after the SSS decrease is not available; in the case of SMOS, we have no information about the duration of the S_{1cm} decrease.

Hence, while the drifter estimate would need to be refined in future studies, in particular by adding other information either coming from ARGO STS [*Anderson and Riser*, 2012] or from drifters measuring roughness in addition to SSS (e.g., SURPACT) [*Reverdin et al*., 2013], it is very interesting to observe that the order of magnitude of S_{45cm} variability associated with rain events is rather consistent with the one of SMOS S_{1cm}.

Given the sparsity of in situ measurements and the lack of SSS measurements under rain events simultaneously by SMOS and in situ, we can not reach a conclusion on the vertical variability between 1 cm and 5 m depth (the typical depth of the ARGO SSS measurements).

In order to further progress on the interpretation of the differences between satellite and ARGO derived salinity products, future experiments should be conducted in rainy regions. They should aim at providing in situ reference with caracteristics similar to the satellite measurements ones. A high temporal sampling is needed to get in situ reference measurements in phase with satellite passes, as well as a vertical sampling between the first top centimeters and several meters depth. It would also be desirable to monitor salinity in several locations within a satellite pixel to enable estimate of in situ salinity averaged at the same resolution as a satellite pixel.

The order of magnitude we find ($\sim$0.2 pss (mm h^{-1}) $^{-1}$) leads to a small effect when applied to one month of data (only -0.2 effect in pixels with a mean monthly RR of 1 mm h^{-1} which is already a large value for mean monthly RR (Figure 1)), and it is at most 40% of the local difference between SMOS S_{1cm} and interpolated ARGO S_{bulk} mapped products (Figure 9) . Hence even if the interpolation of ARGO measurements would miss a part of the rain induced SSS decrease, both because ARGO is measuring bulk salinity and is very undersampled, this cannot explain the whole difference. Other contributions to the difference could be from the spatial interpolation which smoothes spatial gradients, to relaxation to SSS climatology in the mapping algorithm which may overestimate SSS in rainy region, or to remaining SMOS flaws, in particular Radio Frequency Interferences. A correction of -0.2 pss (mm h^{-1}) $^{-1}$ only very slightly reduces the "natural" variability derived from SMOS measurements. In the ITCZ region, it is estimated to be 0.31 from SMOS rain-corrected measurements. This is rather comparable (although 30% higher) to the variability sampled by ARGO (0.24), with or without eliminating measurements at less than 2 h from rain events. This illustrates that, in a very rainy region, even after having taken into account the large S_{1cm} variability occurring at the time of the rainfall, a large variability remains both on SMOS and on in situ bulk measurements. Thus, although vertical stratification between the level of the bulk measurements and the surface could contribute to this variability, a large part of it penetrates deeper than 5 m and is sensed in the bulk Argo data.

Acknowledgements

We thank two anonymous reviewers for their constructive comments. This work is part of the SMOS GLOSCAL Cal/Val project supported by CNES-TOSCA and of the SMOS+SOS STSE study supported by ESA. The US drifters were funded by the NOAA Global Drifter Program grant NA10OAR4320156. L. Centurioni was supported by NOAA grant NA10OAR4320156 and NASA grant NNX12AI67G. We thank Jean-Luc Vergely for very helpful discussions about SMOS theoretical error. We thank Fabienne Gaillard for providing ISAS SSS maps, that are available on request. SSM/I, TMI, AMSR and WindSat data are produced by Remote Sensing Systems and sponsored by the NASA Earth Science MEaSUREs DISCOVER Project. Data are available at www.remss.com. SMOS SSS level 2 are free data set distributed by ESA. Drifter data are available on www.locean-ipsl.upmc.fr/smos/drifters and via http://spurs.jpl.nasa.gov/SPURS/. ARGO data were collected and made freely available by the Coriolis project and programmes that contribute to it (http://www.coriolis.eu.org).

References

Anderson, J., and S. Riser (2012), Near-surface variability of temperature and salinity: Observations from profiling floats, in *Aquarius/SAC-D Science Team Meeting*, Buenos Aires.

Boutin, J., P. Waldteufel, N. Martin, G. Caudal, and E. Dinnat (2004), Surface aalinity retrieved from SMOS measurements over the Global Ocean: Imprecisions due to sea surface roughness and temperature uncertainties, *J. Atmos. Technol.*, *21*(9), 1432–1447.

Boutin, J., N. Martin, Y. Xiaobin, J. Font, N. Reul, and P. Spurgeon (2012), First assessment of SMOS data over open ocean: Part II: Sea surface salinity, *IEEE Trans. Geosci. Remote Sens.*, *50*(5), 1662–1675.

Boutin, J., N. Martin, G. Reverdin, X. Yin, and F. Gaillard (2013), Sea surface freshening inferred from SMOS and ARGO salinity: Impact of rain, *Ocean Sci.*, *9*(1), 183–192.

Carval, T., et al. (2012), Argo User's Manual v2.4, *Rep. reference cor-do/dti-mut/02-084*, 85 pp., Institut Français de Recherche pour l'Exploitation de la Mer (IFREMER), Brest, France.

Durand, F., G. Alory, R. Dussin, and N. Reul (2013), SMOS reveals the signature of Indian Ocean dipole events, *Ocean Dyn.*, *63*(11-12), 1203–1212.

Font, J., A. Camps, A. Borges, M. Martin-Neira, J. Boutin, N. Reul, Y. H. Kerr, A. Hahne, and S. Mecklenburg (2010), SMOS: The challenging sea surface salinity measurement from space, *Proc. IEEE*, *98*(5), s649–s665.

Gaillard, F. (2012), ISAS-Tool version 6: Method and configuration, report LPO-12-02, 18 pp., Laboratoire de Physique des Océans (LPO).

Gordon, A. L., and C. F. Giulivi (2008), Sea surface salinity trends over fifty years within the subtropical North Atlantic, *Oceanography*, *21*(1), 20–29.

Hasson, A., T. Delcroix, and J. Boutin (2013), Formation and variability of the South Pacific sea surface salinity maximum in recent decades, *J. Geophys. Res. Oceans*, *118*, 5109–5116, doi:10.1002/jgrc.20367.

Hasson, A., T. Delcroix, J. Boutin, R. Dussin, and J. Ballabrera-Poy (2014), Analyzing the 2010–2011 La Niña signature in the tropical Pacific sea surface salinity using in situ data, SMOS observations and a numerical simulation, *J. Geophys. Res. Oceans*, *119*, 3855–3867, doi:10.1002/2013JC009388.

Hernandez, O., J. Boutin, N. Kolodziejczyk, G. Reverdin, N. Martin, F. Gaillard, N. Reul, and J. L. Vergely (2014), SMOS salinity in the subtropical North Atlantic salinity maximum: 1. Comparison with Aquarius and in situ Salinity, *J. Geophys. Res. Oceans*, doi:10.1002/2013JC009610, in press.

Hilburn, K. A., and F. J. Wentz (2008), Intercalibrated passive microwave rain products from the Unified Microwave Ocean Retrieval Algorithm (UMORA), *J. Appl. Meteorol. Climatol.*, *47*(3), 778–794.

Kainulainen, J., A. Colliander, J. Closa, M. Martin-Neira, R. Oliva, G. Buenadicha, P. Rubiales Alcaine, A. Hakkarainen, and M. T. Hallikainen (2012), Radiometric performance of the SMOS reference radiometers—Assessment after one year of operation, *IEEE Trans. Geosci. Remote Sens.*, *50*(5), 1367–1383.

Kerr, Y. H., et al. (2010), The SMOS mission: New tool for monitoring key elements of the global water cycle, *Proc. IEEE*, *98*(5), 666–687.

Lagerloef, G. (2012), Satellite mission monitors ocean surface salinity, *Eos Trans. AGU*, *93*(25), 233–240.

Lagerloef, G., et al. (2008), The Aquarius/SAC-D mission: Designed to meet the salinity remote sensing challenge, *Oceanography*, *21*(1), 68–81.

Meissner, T., and F. J. Wentz (2009), Wind-vector retrievals under rain with passive satellite microwave radiometers, *IEEE Trans. Geosci. Remote Sens.*, *47*(9), 3065–3083.

Peichl, M., V. Wittmann, E. Anterrieu, B. Picard, N. Skou, and S. Solbjerg (2004), Scientific inputs for the SMOS Level 1 Processor development, Final report for ESA contract No. 10508/02/NL/GS, DLR, Munich, Germany.

Reul, N., et al. (2013), Sea surface salinity observations from space with the SMOS satellite: A new means to monitor the marine branch of the water cycle, *Surv. Geophys.*, *35*(3), 681–722.

Reverdin, G., S. Morisset, J. Boutin, and N. Martin (2012), Rain-induced variability of near sea-surface T and S from drifter data, *J. Geophys. Res.*, *117*, C02032, doi:10.1029/2011JC007549.

Reverdin, G., S. Morisset, D. Bourras, N. Martin, A. Lourenço, J. Boutin, C. Caudoux, J. Font, and J. Salvador (2013), Surpact: A SMOS Surface Wave Rider for Air-Sea Interaction, *Oceanography*, *26*(1), 48–57.

Reverdin, G., et al. (2014), Validation of surface salinity from drifters, *J. Atmos. Oceanic Technol.*, *31*(4), 967–983.

Rhein, M., et al. (2013), Observations: Ocean, in *Climate Change 2013: The Physical Science Basis. Contribution of Working Group I to the Fifth Assessment Report of the Intergovernmental Panel on Climate Change*, edited by T. F. Stocker, D. Qin, G.-K. Plattner, et al., pp. 255–316, Cambridge Univ. Press, Cambridge, U. K.

Schmitt, R. W. (2008), Salinity and the global water cycle, *Oceanography*, *21*(1), 12–19.

Soloviev, A., and R. Lukas (1996), Observation of spatial variability of diurnal thermocline and rain-formed halocline in the western Pacific warm pool, *J. Phys. Oceanogr.*, *26*(11), 2529–2538.

Tang, W., S. Yueh, A. Fore, G. Neumann, A. Hayashi, and G. Lagerloef (2013), The rain effect on Aquarius' L-band sea surface brightness temperature and radar backscatter, *Remote Sens. Environ.*, *137*, 147–157.

Terray, L., L. Corre, S. Cravatte, T. Delcroix, G. Reverdin, and A. Ribes (2011), Near-surface salinity as nature's rain gauge to detect human influence on the tropical water cycle, *J. Clim.*, *25*(3), 958–977.

Wentz, F. J. (2005), The effect of clouds and rain on the aquarius salinity retrieval, *Remote Sens. Syst. Tech. Memo. 3031805*, Remote Sensing System, Santa Rosa, Calif.

Wentz, F. J. (2013), SSM/I version-7 calibration report, *Rep. 011012*, 46 pp., Remote Sens. Syst., Santa Rosa, Calif.

Yin, X., J. Boutin, and P. Spurgeon (2012a), First assessment of SMOS data over open ocean: Part I;Pacific Ocean, *IEEE Trans. Geosci. Remote Sens.*, *50*(5), 1648–1661.

Yin, X., J. Boutin, N. Martin, and P. Spurgeon (2012b), Optimization of L-band sea surface emissivity models deduced from SMOS data, *IEEE Trans. Geosci. Remote Sens.*, *50*(5), 1414–1426.

Yin, X., J. Boutin, N. Martin, P. Spurgeon, J.-L. Vergely, and F. Gaillard (2013), Errors in SMOS Sea surface salinity and their dependency on a priori wind speed, *Remote Sens. Environ.*, *146*, 159–171, doi:j.rse.2013.09.008.

Zine, S., et al. (2008), Overview of the SMOS sea surface salinity prototype processor, *IEEE Trans. Geosci. Remote Sens.*, *46*, 621–645.